Optics Letters

Detection technique effect on rotational Doppler measurements

Alexander Q. Anderson,[1,*] Elizabeth F. Strong,[2] Brendan M. Heffernan,[3] Mark E. Siemens,[4] Gregory B. Rieker,[2] and Juliet T. Gopinath[1,3]

[1]Department of Electrical, Computer, and Energy Engineering, University of Colorado, Boulder, Colorado 80309, USA
[2]Department of Mechanical Engineering, University of Colorado, Boulder, Colorado 80309, USA
[3]Department of Physics, University of Colorado, Boulder, Colorado 80309, USA
[4]Department of Physics and Astronomy, University of Denver, 2112 East Wesley Avenue, Denver, Colorado 80308, USA
*Corresponding author: alexander.q.anderson@colorado.edu

Received 17 February 2020; revised 1 April 2020; accepted 1 April 2020; posted 3 April 2020 (Doc. ID 390425); published 30 April 2020

There are two established methods for measuring rotational Doppler shift: (1) heterodyne and (2) fringe. We identify a key distinction, that only the heterodyne method is sensitive to the rotating object's phase, which results in significant differences in the signal-to-noise ratio (SNR) when measuring multiple rotating particles. When used to measure randomly distributed rotating particles, the fringe method produces its strongest SNR when a single particle is present and its SNR tends to zero as the number of particles increases, whereas the heterodyne method's SNR increases proportionally to the number of particles in the beam.

https://doi.org/10.1364/OL.390425

Light with orbital angular momentum (OAM) is defined by a helical transverse phase structure [1] described by the azimuthal phase term of $e^{il\phi}$, such that the light has $l\hbar$ of OAM per photon, and ϕ is the azimuthal coordinate. One consequence of this is the rotational Doppler effect (RDE) [2,3]: light scattered from an object rotating about the beam's axis experiences a frequency shift, $\Delta f = \Delta l \Omega / 2\pi$, proportional to the object's angular frequency Ω and the light's change in angular momentum Δl.

The RDE has been proposed as a mechanism for OAM spectrum analysis [4] and for measuring vibration [5], vorticity in fluid flows [6,7], and rotation of remote objects [8] or astronomical sources [9]. The RDE has been observed from optical elements that scatter the incident beam into a particular output OAM state, such as a dove prism [10], spiral phase hologram [11], or Q plate [12], as well as from objects that scatter the incident beam into many different OAM states, such as one or more rotating particles [6,7,13] or a random scattering surface [14]. Regardless of the rotating object, these experiments generally use one of two established techniques to measure the RDE: heterodyne, in which a single OAM mode (donut beam) illuminates the target and interferes with a reference mode; or the fringe method, in which the target is illuminated with two OAM modes of opposite charge, forming a petal beam of azimuthal fringes [Fig. (1)]. Most experiments appear to choose arbitrarily between the detection approaches, as the differences between the approaches and their influence on the experimental outcome are not well-understood.

In this Letter, we identify a key distinction between the heterodyne and fringe methods' signal-to-noise ratio (SNR). We derive and experimentally verify that the heterodyne method is phase sensitive, whereas the fringe method is sensitive only to amplitude modulation. For randomly distributed scattering particles rotating in the beam, we find the fringe method's SNR is strongest when a single particle is present, and it decreases monotonically to zero as the number of particles in the beam increases. In contrast, the heterodyne method's SNR increases linearly as the number of particles in the beam increases. These results are analogous to the findings in the field of laser Doppler velocimetry [15], and provide a useful metric by which a detection method may be chosen based on the density of scatterers in the target medium in order to measure the strongest signal.

We begin by calculating the theoretical photocurrent for an RDE measurement, first for the heterodyne method, then explaining the differences for the fringe method. The heterodyne illumination beam (or probe) is defined as a Laguerre–Gauss (LG) mode with a single topological charge (TC) l. To achieve optimal spatial overlap of these beams on the photodetector, the reference mode is chosen as the $-l$ mode. (The difference in OAM modes, Δl, is thus $2l$.) The form of both beams is given by Eq. (1), where $f(r)$ represents the modes' radial profile and normalization factors as defined for Laguerre–Gaussian beams,

$$E(r, \phi, t) = A f(r) e^{i(\omega t - l\phi)}. \tag{1}$$

The rotating object may be equivalently represented either as a superposition of many TCs and radial modes, or as a distribution of particles, each with a different depth (corresponding to phase difference) and/or reflectivity. The effect of an object's TCs on the RDE signal has been studied elsewhere [11,16]; however, for sensing applications such as lidar and microscopy, in which a rotating target may comprise one or more particles in the beam, a more natural basis is to instead decompose such targets as a distribution of particles. The RDE frequency shift

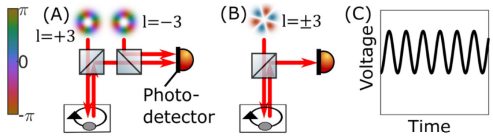

Fig. 1. Rotational Doppler shift measurement techniques: (A) A single OAM mode illuminates a spinning object and is heterodyned with a reference of a different OAM value. (B) A petal beam illuminates a spinning object, providing amplitude modulation. (C) Both methods generate a beat frequency at $\Delta l\Omega/2\pi$.

depends only on the angular distribution of particles [11]; whereas the effect of the radial distribution primarily decreases the measurement's light collection efficiency. We therefore model the particles as wedges of uniform angular width θ_p and infinite radial extent. Additionally, we assume the particles have a uniform reflectivity of R; since R only scales the RDE signal, we set R to 1 for simplicity. To consider the effect of multiple particles in the beam, we represent the rotating object's complex reflectivity, P, as a sum of contributions from N nonoverlapping particles rotating about the origin with an angular frequency of Ω, each with an azimuthal position at time 0 of θ_m, and a phase, ψ_m, corresponding to the axial position of the particle,

$$P(\phi, t) = \sum_{m=1}^{N} \begin{cases} e^{i\psi_m} & \Omega t + \theta_m < \phi < \theta_p + \Omega t + \theta_m \\ 0 & \text{otherwise} \end{cases}. \quad (2)$$

The photocurrent is calculated by integrating the power incident on the detector. The illumination beam E_i is multiplied by the rotating target function, P, then imaged onto the reference beam E_r at the detector, which sums the total incident intensity,

$$i(t) = \kappa \int_0^{R_d} \int_0^{2\pi} (E_i P + E_r)(E_i P + E_r)^* r \mathrm{d}\phi \mathrm{d}r. \quad (3)$$

Subscripts i and r represent incident and reference beam quantities, respectively, and κ is a constant dependent on the system losses and detector sensitivity. When evaluating Eq. (3), we assume that the beams underfill the detector of radius R_d. Because the reference beam mode is chosen as $l_r = -l_i$, the radial integral simply evaluates to $1/2\pi$ (a different choice of reference mode would decrease the signal due to decreasing spatial overlap of the reference and probe; a particle of limited radial extent would likewise decrease the signal). Calculating the heterodyne photocurrent [Eq. (4)] reveals that each individual rotating particle contributes a signal of the same frequency $\Delta l\Omega/2\pi$ but with a phase originating from the particle's position θ_m and its phase ψ_m,

$$i(t) = \kappa \left(|A_r|^2 + \frac{N\theta_p}{2\pi}|A_i|^2 + A_i A_r^* \frac{2}{\pi \Delta l} \sin\left(\frac{\Delta l \theta_p}{2}\right) \times \sum_m^N \cos\left(\Delta l(\Omega t + \theta_m) + \psi_m\right) \right). \quad (4)$$

Calculating the photocurrent for the fringe method requires a few changes. The fringe method's probe consists of two OAM modes of $+l$ and $-l$ (Δl is again $2l$), forming a petal beam of azimuthal fringes,

$$E(r, \phi, t) = Af(r)\left(e^{i(\omega t - l\phi)} + e^{i(\omega t + l\phi)}\right). \quad (5)$$

The fringe method does not use a reference beam, so E_r is set to zero. Evaluating Eq. (3) results in a photocurrent for the fringe method [Eq. (6)], which is similar to that of the heterodyne method, again summing a sinusoidal signal from each individual particle.

$$i(t) = \frac{\kappa |A_i|^2}{\pi} \left[N\theta_p + \frac{2}{\Delta l} \sin\left(\frac{\Delta l \theta_p}{2}\right) \sum_m^N \cos(\Delta l(\Omega t + \theta_m)) \right]. \quad (6)$$

However, Eq. (6) is independent of particle phase ψ_m; this reveals the fringe method is sensitive only to the amplitude modulation of the particle distribution, and not to the phase modulation it provides. Both the fringe [Eq. (6)] and heterodyne [Eq. (4)] methods measure a beat at $\Delta l\Omega/2\pi$, usually explained as arising from frequency shifts in scattered modes of the probe beam, proportional to the mode's change in OAM [14]. An equivalent explanation for fringe method's beat is the amplitude modulation from a particle traversing the petal beam's angular fringes.

We designed an experiment to measure the RDE using both heterodyne and fringe methods to highlight specific cases of how phase sensitivity affects the measurements. As shown in Fig. 2, a He–Ne laser is spatially filtered then prepared by a spatial light modulator [17] (SLM, modified Epson EMP83 projector) as either an $l = -3$ donut beam or $l = \pm 3$ petal beam for heterodyne and fringe methods, respectively. The beam then diffracts from a second SLM (Cambridge Correlator SDE1024), which emulates a rotating object by spinning a computer-generated hologram (CGH) at angular frequency Ω. To implement this CGH, the desired object's complex reflectivity is multiplied by a sine grating; the object term rotates as a video while the grating remains static to maintain a constant direction of the diffracted mode. Using an SLM rather than a physical scattering target allows precise, dynamic control over the target and simplifies axial alignment between the beam and the rotating object.

Following the holographically emulated rotating object on the SLM, a beam splitter directs the reflected beam to the photodetector (Thorlabs Det36A). For the heterodyne method, a reference beam is reflected from the beam splitter following the first SLM and has its parity reversed to $l = +3$ by an extra reflection before recombining with the probe. The reference

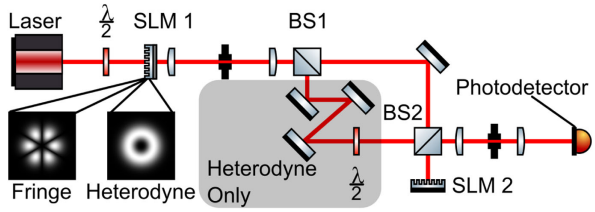

Fig. 2. Layout of RDE experiment. A spatial light modulator (SLM1) prepares the incident beam, either as a petal beam or a donut beam for fringe or heterodyne methods, respectively. The probe beam transmits through both beam splitters (BS), scatters from a rotating object simulated on SLM2, then returns to BS2, where a telescope images it to the photodetector. For the heterodyne method, the reference beam comes from the reflection of BS1, which is then path length matched and has the OAM parity reversed before recombining at BS2. This reference path is blocked for the fringe method. Telescopes with spatial filters follow both SLMs to select the proper diffracted mode.

and probe beams must be precisely collinearly aligned to mode match, as misalignment results in a broadened OAM spectrum [18]. Due to the tight tolerances for this alignment [18], a camera and a wavefront sensor were used to match the reference and probe beams' centroids and wavefront tilts. The power spectral density (PSD) of the resulting photocurrent is calculated using Welch's method with a Hann window for smoothing, with the expected beat frequency at $\Delta l\Omega/2\pi$, where Δl is 6 for both techniques.

Three rotating holograms were implemented [Fig. 3 insets]. Two of these holograms produce the same amplitude modulation of six equally spaced, wedge-shaped particles of angular width $\pi/6$, but with different phase conditions on consecutive particles. Hologram 1 [Fig. 3A inset] has a uniform phase on all the particles, and hologram 2 [Fig. 3B inset] has alternating 0 and π phases on consecutive particles. The third hologram [Fig. 3C inset] emulates 12 particles with alternating 0 and π phases, filling the beam. These holograms were all rotated at a frequency of 0.11 Hz, limited by the refresh rate of the SLM.

The measured PSD from each hologram is shown in Fig. 3. Because the fringe method measures only amplitude modulation, it produces the same signal for both six-particle holograms despite their different phase conditions, but no signal is measured in the 12 particle case, as this hologram has no amplitude variation. In contrast, the heterodyne detection yields a strong signal for both the 12-particle hologram and the uniform-phase six-particle hologram [Fig. 3C, 3A]. However, the heterodyne method does not produce a signal from the second six-particle hologram [Fig. 3B] because it is phase sensitive and each pair of particles in this hologram produces equal and opposite signals that destructively interfere. Clearly, the amplitude and phase sensitivity of the fringe and heterodyne techniques are important factors to consider when designing an RDE measurement system.

Another important consideration is the effect of misalignment. In either method, misalignment of the illumination beam from the rotation axis will broaden the beam's effective OAM spectrum [18], yielding multiple Δl values between the optical modes. This then generates many discrete frequency shifts of $\Delta l_n\Omega/2\pi$, rather than a single pure frequency shift [18,19]. The heterodyne method additionally requires precise alignment

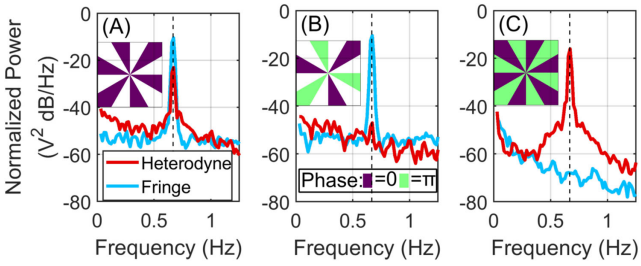

Fig. 3. Power spectral densities of measured time series for fringe and heterodyne methods for three different rotating holograms (insets). Hologram color depicts emulated particles' phase; white indicates absence of particle (zero reflectivity). The holograms' sinusoidal modulation is not shown. At the expected frequency of $f = 0.67$ Hz (dashed), the fringe method produces a signal for (A), (B) both six-particle rotating objects, despite the differing phase conditions, but produces no signal for (C) the 12-particle hologram, as the target displays no amplitude modulation. The phase sensitivity of the heterodyne method gives rise to a strong signal for case C but does not generate a signal for case B due to destructive interference.

of the reference beam with the scattered probe in order to mode match to again prevent broadening of the effective OAM spectrum. Because the fringe method generates both modes of the petal beam simultaneously from the same hologram, it does not require this additional alignment, so the fringe method is significantly easier to align.

In most applications, rotating particles are likely to be randomly spaced in the beam, with their random axial positions corresponding to random phases. Using the same model and assumptions as above, we now show that the difference in phase sensitivity results in a change in behavior in the expectation values of the SNRs for the two methods when measuring randomly distributed particles. We first show that the heterodyne method's SNR increases linearly with the number of random particles in the beam, N, and then show that the fringe method's SNR monotonically decreases to zero as the N increases. We will assume each particle's phase, ψ_m, is random and independent, and its azimuthal position, θ_m, is random but constrained to prevent particles from occupying the same space.

Consider the photocurrent generated in the heterodyne method [Eq. (4)]. Each particle contributes a sinusoidal term with its phase dependent on both ψ_m, and θ_m; for each particle, these two random phases can be summed to a single independent, random phase, ψ'_m, distributed uniformly modulo 2π. With this definition of ψ'_m, the expected photocurrent for N random, rotating particles is found [Eq. (7)] by applying the expectation value of a sum of randomly phased sinusoids [Eq. (8)], which yields an expected amplitude of $\sqrt{N\pi/4}$, but maintains the same frequency content (a full derivation of this expectation value is given in [20]),

$$E[i(t)] = \kappa\left(A_r^2 + \frac{N\theta_p}{2\pi}A_i^2 + \frac{\sqrt{N}A_iA_r^*}{\sqrt{\pi}\Delta l}\sin\left(\frac{\Delta l\theta_p}{2}\right) \times \cos(\Delta l\Omega t)\right), \tag{7}$$

$$E\left[\sum_{m=1}^{N}\cos(\omega t + \psi'_m)\right] = \sqrt{N\frac{\pi}{4}}\cos(\omega t). \tag{8}$$

To predict the expected SNR, we assume the measurement is signal shot-noise limited. Due to both the phase sensitivity and the heterodyne gain, the SNR is directly proportional to the number of random particles in the beam [Eq. (9)],

$$\mathrm{SNR_{het}} = \left(\frac{\mathrm{AC_{signal}}}{\sqrt{\mathrm{DC_{signal}}}}\right)^2 = \frac{\kappa N|A_i|^2|A_r|^2\frac{1}{\pi(\Delta l)^2}\sin^2\left(\frac{(\Delta l\theta_p)}{2}\right)}{|A_r|^2 + \frac{N\theta_p}{2\pi}|A_i|^2}. \tag{9}$$

This SNR is plotted in Fig. 4 as a function of fill factor $N\theta_p/2\pi$, a dimensionless measure of the total area the particles occupy.

We next consider the fringe technique, returning to the photocurrent calculated in Eq. (6). As previously discussed, this measurement is not sensitive to the particles' random phases; thus, while each particle still produces a randomly phased signal of frequency $\Delta l\Omega/2\pi$, the random phases of these photocurrent terms depend only on each particle's angular position θ_m. While these positions are random, two particles cannot be in the same place, so the random positions, and therefore the random phases of the photocurrent terms, are not independently

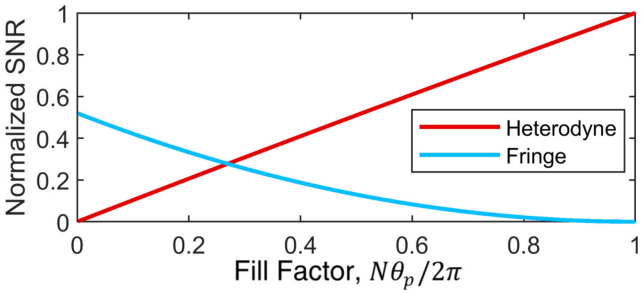

Fig. 4. Theoretically calculated SNR of rotational Doppler effect signal for N randomly distributed, wedge-shaped particles with random phases rotating about the origin, for both techniques [Eqs. (9) and (12)]. Results are normalized to the peak value of the heterodyne curve. The particle angular width is fixed at $\theta_p = 0.01$, $\Delta l = 6$, and $A_r = 5A_i$ for heterodyne. Fill factor is defined as the percent of the angular area of the beam covered by the particles. The fringe SNR is best for few particles in the beam, but the heterodyne SNR increases with N.

random. Thus, the expectation value of Eq. (8) is not valid. Because the overlap constraint becomes more significant as the particles fill the beam, the expectation value should converge to Eq. (8) when the fill factor $N\theta_p/2\pi$ is small, but as the fill factor increases, the amplitude should eventually decrease to 0. A simple correction factor proportional to the fill factor was postulated and verified by fitting to simulated random trials of summing sine waves with random phases; the simulated trials were fit as Eq. (10) with an R^2 of 0.9975 for small angles ($\theta_p < 0.1$) and for $N > 1$,

$$E[A] = \sqrt{\frac{\pi}{4}N}\left(1 - N\frac{\theta_p}{2\pi}\right). \tag{10}$$

Using these results, the expected photocurrent using the fringe method to measure N random particles is given as

$$E[i(t)] = \frac{\kappa|A_i|^2}{\pi}\left[N\theta_p + \frac{\sqrt{N\pi}}{\Delta l}\left(1 - N\frac{\theta_p}{2\pi}\right) \times \sin\left(\frac{\Delta l\theta_p}{2}\right)\cos(\Delta l\Omega t)\right]. \tag{11}$$

Using the same assumption that the measurement is shot noise limited, the SNR is given by

$$\mathrm{SNR}_{\mathrm{fringe}} = \frac{\kappa|A_i|^2}{\theta_p(\Delta l)^2}\left(1 - \frac{N\theta_p}{2\pi}\right)^2 \sin^2\left(\frac{\Delta l\theta_p}{2}\right). \tag{12}$$

As shown in Fig. 4, the fringe method produces a strong signal when few random particles are present, but its SNR decreases as $O(N^2)$, whereas the heterodyne method's SNR increases linearly with N (assuming the reference beam has much more power than the probe beam). When the beam is fully filled with particles, the fringe method's SNR is zero, while the heterodyne method measures a strong signal due to its phase sensitivity. The difference in techniques is even more pronounced if a minor amount of background noise is considered in the calculations, due to the effect of heterodyne gain.

A careful analysis of the two RDE measurement techniques shows that only the heterodyne method is phase sensitive, which makes it better suited to large numbers of randomly distributed rotating particles. While both methods generate signals at the same frequency, they are most sensitive in opposite conditions: the fringe method is best with a single particle whereas the heterodyne SNR increases with the number of particles. The density of scatterers in the rotating target is thus an essential parameter to consider when designing a system to measure rotation with the RDE. When considered along with the differences in alignment requirements, these physical and practical considerations enable an RDE measurement to be better understood and optimized, for applications in fluid dynamics, astronomy, and remote sensing.

Funding. National Defense Science and Engineering Graduate; National Science Foundation (DGE 1650115, DMR 1553905, ECCS 1509733, ECCS 1509928, ECCS 1554704); Air Force Office of Scientific Research (FA9550-17-1-0224); University of Colorado Boulder (Seed Grant Program) Department of Electrical, Computer, and Energy Engineering at University of Colorado Boulder.

Acknowledgment. We thank Dr. Gabriel Molina-Terriza, Dr. Aniceto Belmonte, Dr. Martin Lavery, and Dr. Mike Wardlaw for helpful technical discussions.

Disclosures. The authors declare no conflicts of interest.

REFERENCES

1. L. Allen, M. W. Beijersbergen, R. J. C. Spreeuw, and J. P. Woerdman, Phys. Rev. A **45**, 8185 (1992).
2. L. Allen, M. Babiker, and W. L. Power, Opt. Commun. **112**, 141 (1994).
3. M. J. Padgett, J. Opt. A **6**, S263 (2004).
4. H. L. Zhou, D. Z. Fu, J. J. Dong, P. Zhang, D. X. Chen, X. L. Cai, F. L. Li, and X. L. Zhang, Light Sci. Appl. **6**, e16251 (2017).
5. S. Xiao, L. Zhang, D. Wei, F. Liu, Y. Zhang, and M. Xiao, Opt. Express **26**, 1997 (2018).
6. A. Belmonte, C. Rosales-Guzmán, and J. P. Torres, Optica **2**, 1002 (2015).
7. A. Ryabtsev, S. Pouya, A. Safaripour, M. Koochesfahani, and M. Dantus, Opt. Express **24**, 11762 (2016).
8. W. Zhang, J. Gao, D. Zhang, Y. He, T. Xu, R. Fickler, and L. Chen, Phys. Rev. Appl. **10**, 044014 (2018).
9. R. Neo, S. Leon-Saval, J. Bland-Hawthorn, and G. Molina-Terriza, Opt. Express **25**, 21159 (2017).
10. J. Courtial, K. Dholakia, D. A. Robertson, L. Allen, and M. J. Padgett, Phys. Rev. Lett. **80**, 3217 (1998).
11. H. Zhou, D. Fu, J. Dong, P. Zhang, and X. Zhang, Opt. Express **24**, 10050 (2016).
12. P. Georgi, C. Schlickriede, G. Li, S. Zhang, and T. Zentgraf, Optica **4**, 1000 (2017).
13. M. V. Vasnetsov, J. P. Torres, D. V. Petrov, and L. Torner, Opt. Lett. **28**, 2285 (2003).
14. M. P. J. Lavery, F. C. Speirits, S. M. Barnett, and M. J. Padgett, Science **341**, 537 (2013).
15. L. E. Drain, J. Phys. D **5**, 481 (1972).
16. L. Fang, M. J. Padgett, and J. Wang, Laser Photon. Rev. **11**, 1700183 (2017).
17. V. Arrizón, U. Ruiz, R. Carrada, and L. A. González, J. Opt. Soc. Am. A **24**, 3500 (2007).
18. M. V. Vasnetsov, V. A. Pas'ko, and M. S. Soskin, New J. Phys. **7**, 46 (2005).
19. S. Qiu, T. Liu, Y. Ren, Z. Li, C. Wang, and Q. Shao, Opt. Express **27**, 24781 (2019).
20. J. W. Goodman, *Statistical Optics* (Wiley, 2015).